AIAA 82-4059

Trapping of a Free Vortex by Joukowski Airfoils

Ming-Ke Huang* and Chuen-Yen Chow†
University of Colorado, Boulder, Colo.

The ability of trapping a free vortex by a Joukowski airfoil in its vicinity for lift augmentation is investigated through a two-dimensional potential flow analysis. The effects of angle of attack, thickness, and camber on the trapping performance of the airfoil are examined separately. It is found that to capture a vortex which is stable to small disturbances, the proper arrangement is to have a rather thick symmetric airfoil at a small angle of attack.

I. Introduction

THE lift on a wing can be enhanced by placing an organized vortex in the vicinity of the wing. A well-known example is the additional lift produced by the vortex sheets rolling up along leading edges of a delta wing flying at large angles of attack. Spanwise vortices could be generated and maintained on the upper surface of a large-aspect-ratio wing by deploying some specially designed flaps, as suggested by Kasper[1] who claimed that a lift coefficient of 3.15 had been achieved by a glider based on such a design. Despite the contradictory results from different wind tunnel tests of the Kasper wing,[2,3] Rossow[4] demonstrated, both analytically and experimentally, that it was possible to trap a spanwise vortex over the upper surface of a wing by using a vertical flap near the leading edge while a suction was applied along the vortex axis. The lift coefficient of such a wing could reach as high as 10 with a proper combination of the flap configuration and the suction strength.

As shown by experimental data,[2,3] a large increase in drag is inevitably accompanied with augmented lift when flaps are used to maintain the vortex in a realistic viscous fluid. This drag is expected to diminish with decreasing flap size. Saffman and Sheffield[5] made an analysis of a flat-plate airfoil, which showed that at suitable locations a line vortex might become stationary relative to the airfoil without the help of flaps. The vortex was stable to small disturbances at some of the equilibrium locations, and according to their theoretical investigation, the vortex-augmented lift was significant. Sheffield[6] also examined the vortex-trapping abilities of some Joukowski airfoil profiles.

The works of Saffman and Sheffield[5,6] suggest utilizing the geometry of the airfoil as a method of capturing a line vortex for generation of high lift. This method is relatively simple and, unlike the Kasper's method involving additional flaps, will not cause a tremendous increase of drag on the wing when flying through a viscous fluid. In the present work we consider a general Joukowski airfoil and make an extensive study on the effects of angle of attack, thickness, and camber on the vortex-trapping capability of the airfoil, in the hope of finding some criteria for designing airfoils which efficiently generate high vortex lift.

The sketches in Fig. 1 explain how an external vortex can increase the lift on an airfoil. Figure 1a shows an airfoil flying at speed U through an incompressible fluid of density ρ. To satisfy the Kutta condition at the sharp trailing edge, a circulation Γ is created around the airfoil, which gives rise to a lift of $\rho U\Gamma$ per unit span of the wing. When a vortex of circulation κ is placed above the airfoil, it induces a reversed fluid motion on the upper surface, so that a stagnation point would appear there if the same circulation were maintained around the airfoil. The flow pattern is sketched in Fig. 1b. However, to remove the infinite-velocity situation at the sharp edge, additional circulation $\Delta\Gamma$ has to be generated to shift the stagnation point back to the trailing edge so the Kutta condition is fulfilled again. A vortex of circulation $-\Delta\Gamma$ is shed in the wake as shown in Fig. 1c, and the wing has thus gained a lift of $\rho U(\Delta\Gamma+\kappa)$ per unit span. The dependence of the increased lift on the strength and position of the vortex is one of the main concerns of the present work.

When the steady state for a given airfoil configuration has been reached, we determine the stationary equilibrium locations of the external vortex and compute the associated lift. Furthermore, the stability of the vortex at each of its equilibrium positions is examined. Our analysis is made for a steady two-dimensional flow past an airfoil, under the assumption that the fluid is inviscid and incompressible. The vortex-induced drag cannot be computed using this model.

II. Flow about Joukowski Airfoil

Referring to Fig. 2, we consider the transformations

$$z=\frac{1}{2}\left(\zeta+\frac{1}{\zeta}\right) \tag{1}$$

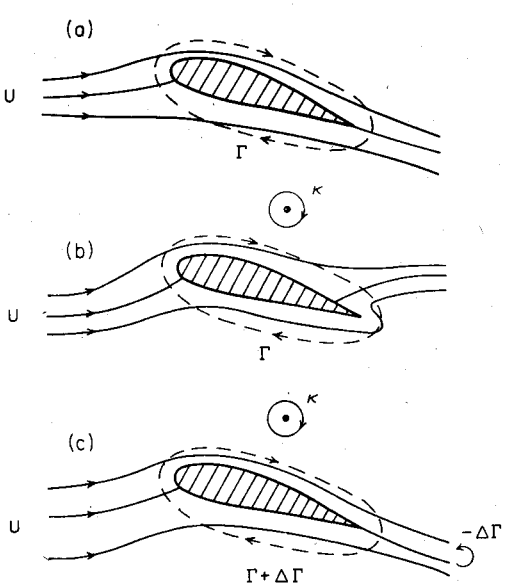

Fig. 1 Flow about an airfoil: a) in the absence of an external vortex, b) in the presence of an external vortex but keeping the same circulation around the airfoil, c) in the presence of an external vortex with the Kutta condition satisfied at the sharp trailing edge.

Received Feb. 3, 1981; revision received Aug. 17, 1981.

*Visiting Scholar, Department of Aerospace Engineering Sciences.
†Professor of Aerospace Engineering Sciences. Member AIAA.

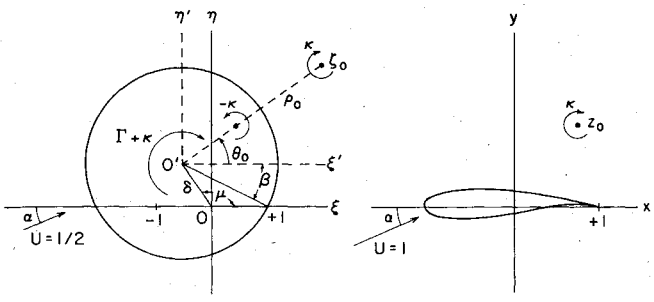

Fig. 2 Transformation of the flow about a circle in the ζ plane into that about an airfoil in the z plane.

$$\zeta=\zeta'+\delta e^{i\mu} \tag{2}$$

in which $z=x+iy$, $\zeta=\xi+i\eta$, and $\zeta'=\xi'+i\eta'$ are complex variables. These transformations map the circle of radius a centered at the origin of the ζ' plane into a Joukowski airfoil in the physical z plane, whose chord is generally greater than 2 but is equal to 2 when the airfoil has the form of a flat plate. In particular, the point $\zeta=1$ is mapped into the sharp trailing edge of the airfoil. The shape of the airfoil is controlled by varying the parameters δ and μ. For example, the generally cambered airfoil becomes a symmetric airfoil when $\mu=\pi$, it becomes a circular arc when $\mu=\pi/2$, and it reduces to a flat plate if $\delta=0$. The radius a of the circle and the angle β shown in Fig. 2 can be expressed in terms of these two parameters as

$$a=\sqrt{1-2\delta\cos\mu+\delta^2} \tag{3}$$

$$\beta=\tan^{-1}\left(\frac{\delta\sin\mu}{1-\delta\cos\mu}\right) \tag{4}$$

These expressions will be used in the later analysis.

Under the same transformations between ζ and z planes, a uniform flow of speed $U=\frac{1}{2}$ making an angle α with the horizontal axis maps into a uniform flow of speed $U=1$ without changing its orientation; and a vortex of circulation κ at ζ_0 maps into a vortex of the same strength situated at z_0, where

$$\zeta_0=\zeta_0'+\delta e^{i\mu} \tag{5}$$

$$\zeta_0'=\rho_0 e^{i\theta_0} \tag{6}$$

Let $w=\Phi+i\Psi$ be the complex potential of the flow, in which Φ is the velocity potential and Ψ is the stream function. The complex potential is first written in the ζ' plane, which consists of the contributions from the uniform flow, the vortex and its image in the circle, and the circulation about the center of the circle.

$$w=\frac{1}{2}e^{-i\alpha}\left(\zeta'+\frac{a^2}{\zeta'}e^{i2\alpha}\right)+\frac{i\kappa}{2\pi}\left[\log(\zeta'-\zeta_0')\right.$$
$$\left.-\log(\zeta'-a^2/\bar{\zeta}_0')\right]+\frac{i}{2\pi}(\Gamma+\kappa)\log\zeta' \tag{7}$$

in which a bar is used to denote the complex conjugate.

The complex velocity of the flow about the airfoil is then derived from Eq. (7)

$$\frac{dw}{dz}=\frac{dw}{d\zeta'}\frac{d\zeta'}{d\zeta}\frac{d\zeta}{dz}=\frac{dw}{d\zeta'}\Big/\frac{dz}{d\zeta} \tag{8}$$

where

$$\frac{dw}{d\zeta'}=\frac{1}{2}e^{-i\alpha}-\frac{1}{2}\left(\frac{a}{\zeta'}\right)^2e^{i\alpha}+\frac{i\kappa}{2\pi}\left[\frac{1}{\zeta'-\zeta_0'}-\frac{1}{\zeta'-a^2/\bar{\zeta}_0'}\right]$$
$$+\frac{i}{2\pi}\frac{\Gamma+\kappa}{\zeta'} \tag{9}$$

$$\frac{dz}{d\zeta}=\frac{\zeta^2-1}{2\zeta^2} \tag{10}$$

Our mathematical problem is now stated as follows. For a given airfoil (with specified δ and μ) at a given angle of attack α, we will determine the position z_0 $(=x_0+iy_0)$ and the strength κ of the free vortex and the circulation Γ around the airfoil, under the constraint that the vortex becomes stationary and the Kutta condition is satisfied at the trailing edge of the airfoil. Note that the Γ described here is equivalent to the sum $\Gamma+\Delta\Gamma$ in Fig. 1c in the steady state when the wake vortex is carried to infinity.

III. Condition for the Free Vortex to Become Stationary

The complex velocity of the free vortex is

$$(u-iv)_{z_0}=\left(\frac{dw}{dz}-\frac{i\kappa}{2\pi}\frac{1}{z-z_0}\right)_{\zeta'=\zeta_0'}$$
$$=\frac{\zeta_0'^2}{\zeta_0'^2-1}\left[e^{-i\alpha}-\left(\frac{a}{\zeta_0'}\right)^2e^{i\alpha}-\frac{i\kappa}{\pi}\frac{1}{\zeta_0'-a^2/\bar{\zeta}_0'}+\frac{i}{\pi}\frac{\Gamma+\kappa}{\zeta_0'}\right]$$
$$+\frac{i\kappa}{2\pi}\left[\frac{1}{\zeta'-\zeta_0'}\frac{d\zeta'}{dz}-\frac{1}{z-z_0}\right]_{\zeta'=\zeta_0'} \tag{11}$$

Taylor's series expansion about the point ζ_0' results in

$$\frac{d\zeta'}{dz}=\left(\frac{d\zeta'}{dz}\right)_0-\left(\frac{d^2z}{d\zeta'^2}\right)_0\left(\frac{d\zeta'}{dz}\right)_0^2(\zeta'-\zeta_0')+0(\zeta'-\zeta_0')^2$$

$$\frac{1}{z-z_0}=\left(\frac{d\zeta'}{dz}\right)_0\frac{1}{\zeta'-\zeta_0'}-\frac{1}{2}\left(\frac{d^2z}{d\zeta'^2}\right)_0\left(\frac{d\zeta'}{dz}\right)_0^2+0(\zeta'-\zeta_0')$$

which give the limiting value of $-2\zeta_0/(\zeta_0^2-1)^2$ for the expression contained within the second square brackets in Eq. (11).

To require that the vortex be stationary we obtain, by equating the right-hand side of Eq. (11) to zero,

$$\zeta_0e^{-i\alpha}-\zeta_0\left(\frac{a}{\zeta_0'}\right)^2e^{i\alpha}+\frac{i\Gamma}{\pi}\frac{\zeta_0}{\zeta_0'}$$
$$+\frac{i\kappa}{\pi}\left[\frac{\zeta_0}{\zeta_0'}\left(1-\frac{1}{1-a^2/|\zeta_0'|^2}\right)-\frac{1}{\zeta_0^2-1}\right]=0 \tag{12}$$

After substituting ζ_0 and ζ_0' from Eqs. (5) and (6) and separating it into real and imaginary parts, Eq. (12) becomes

$$R_1+\frac{\Gamma}{\pi}R_2+\frac{\kappa}{\pi}R_3=0 \tag{13}$$

$$I_1+\frac{\Gamma}{\pi}I_2+\frac{\kappa}{\pi}I_3=0 \tag{14}$$

in which

$$R_1=\left(\rho_0-\frac{a^2}{\rho_0}\right)\cos(\theta_0-\alpha)+\delta\cos(\mu-\alpha)$$
$$-\frac{\delta a^2}{\rho_0^2}\cos(\alpha+\mu-2\theta_0) \tag{15}$$

$$R_2=-\frac{\delta}{\rho_0}\sin(\mu-\theta_0) \tag{16}$$

$$R_3=\frac{\delta a^2}{\rho_0(\rho_0^2-a^2)}\sin(\mu-\theta_0)-\frac{1}{2}\left(\frac{1}{S_1}-\frac{1}{S_2}\right)$$
$$\times(\rho_0\sin\theta_0+\delta\sin\mu) \tag{17}$$

$$I_1=(\rho_0+\frac{a^2}{\rho_0})\sin(\theta_0-\alpha)+\delta\sin(\mu-\alpha)$$
$$-\frac{\delta a^2}{\rho_0^2}\sin(\alpha+\mu-2\theta_0) \quad (18)$$

$$I_2=1+\frac{\delta}{\rho_0}\cos(\mu-\theta_0) \quad (19)$$

$$I_3=-\frac{a^2}{\rho_0^2-a^2}\left[1+\frac{\delta}{\rho_0}\cos(\mu-\theta_0)\right]-\frac{1}{2}\left(\frac{1}{S_1}-\frac{1}{S_2}\right)$$
$$\times(\rho_0\cos\theta_0+\delta\sin\mu)+\frac{1}{2}\left(\frac{1}{S_1}+\frac{1}{S_2}\right) \quad (20)$$

where

$$S_1=1+\rho_0^2+\delta^2+2\rho_0\delta\cos(\mu-\theta_0)-2\rho_0\cos\theta_0-2\delta\cos\mu \quad (21)$$

$$S_2=1+\rho_0^2+\delta^2+2\rho_0\delta\cos(\mu-\theta_0)+2\rho_0\cos\theta_0+2\delta\cos\mu \quad (22)$$

IV. Kutta Condition at the Trailing Edge

The Joukowski airfoil has a cusp at the trailing edge where the upper and lower surfaces are tangent. The Kutta condition for this type of edge is that the velocity there is finite. It demands in Eq. (8) that $dw/d\zeta'=0$ at $\zeta=1$, that is, at $\zeta'=ae^{-i\beta}$ as indicated in Fig. 2. Starting from Eq. (9) and after some manipulation, this requirement becomes

$$\sin(\alpha+\beta)=\frac{\Gamma+\kappa}{2\pi a}-\frac{\kappa}{\pi}F \quad (23)$$

where

$$F=-\tfrac{1}{2}e^{-i\beta}\left(\frac{1}{\zeta'-\zeta_0'}-\frac{1}{\zeta'-a^2/\bar{\zeta}_0'}\right)_{\zeta'=ae^{-i\beta}}$$
$$=\frac{\rho_0^2-a^2}{2a[\rho_0^2+a^2-2a\rho_0\cos(\theta_0+\beta)]} \quad (24)$$

Let us go one step further to compute the velocity at the trailing edge where the right-hand side of Eq. (8) has the indeterminate form. The complex velocity at the trailing edge is then evaluated accordingly.

$$(u-iv)_{z=1}=\left(\frac{d^2w}{d\zeta'^2}\Big/\frac{d^2z}{d\zeta'^2}\right)_{\zeta'=ae^{-i\beta}}$$
$$=\left[\frac{a^2}{\zeta'^3}e^{i\alpha}-i\frac{\Gamma+\kappa}{2\pi\zeta'^2}-\frac{i\kappa}{2\pi}\left(\frac{1}{\zeta'-\zeta_0'}-\frac{1}{\zeta'-a^2/\bar{\zeta}_0'}\right)\right.$$
$$\left.\times\left(\frac{1}{\zeta'-\zeta_0'}+\frac{1}{\zeta'-a^2/\bar{\zeta}_0'}\right)\right]_{\zeta'=ae^{-i\beta}} \quad (25)$$

The expression is obtained by differentiating Eqs. (9) and (10) and by using the fact that $d^2z/d\zeta^2=1$ at $\zeta=1$. After simplified by the use of Eqs. (23) and (24), the result reveals that the velocity at the trailing edge makes an angle -2β with the x axis and has a magnitude

$$V_t=\frac{\cos(\alpha+\beta)}{a}-\frac{2\rho_0\sin(\theta_0+\beta)}{\rho_0^2+a^2-2a\rho_0\cos(\theta_0+\beta)}$$
$$\times\left[\frac{\Gamma+\kappa}{2\pi a}-\sin(\alpha+\beta)\right] \quad (26)$$

A negative value of V_t means the direction of the flow at the trailing edge is from the trailing to the leading edge, which is in contradiction to the situation in the present flow problem. Thus the solution corresponding to $V_t<0$ is thrown away even if it satisfies the Kutta condition represented by Eq. (23).

V. Method of Solution

We now have three algebraic equations, Eqs. (13), (14), and (23), for three of the four unknowns κ, Γ, ρ_0, and θ_0. The system of equations can be rearranged in a more convenient form. Equations (13) and (14) are first combined to obtain

$$\frac{\Gamma}{\pi}=-\frac{R_1I_3-R_3I_1}{R_2I_3-R_3I_2} \quad (27)$$

$$\frac{\kappa}{\pi}=-\frac{R_1}{R_3}-\frac{\Gamma R_2}{\pi R_3} \quad (28)$$

Upon substitution into Eq. (23) a single equation results

$$\sin(\alpha+\beta)+\frac{1}{2a}\frac{R_1I_3-R_3I_1}{R_2I_3-R_3I_2}+\left(\frac{1}{2a}-F\right)$$
$$\times\left(\frac{R_1}{R_3}-\frac{R_2}{R_3}\cdot\frac{R_1I_3-R_3I_1}{R_2I_3-R_3I_2}\right)=0 \quad (29)$$

which contains only two variables ρ_0 and θ_0. The problem is solved according to the following procedure.

For a set of assumed values of α, δ, and μ, the values of a and β are calculated from Eqs. (3) and (4), and the airfoil shape is drawn by mapping the circle of radius a at the origin of the ζ' plane through the transformations Eqs. (1) and (2). We look for all possible locations at which a free vortex becomes stationary by searching along the radial direction for each of the many values of θ_0 selected between 0 and 2π. For a given value of θ_0, if no value of ρ_0 can be found that will satisfy Eq. (29), it means that no vortex can be trapped in that direction. Otherwise, the coordinates (ρ_0, θ_0) thus found are used to compute the values of Γ and κ from Eqs. (27) and (28) and to determine the position (x_0, y_0) of the vortex in the physical plane using Eqs. (1) and (2). Loci of the free vortex for both constant α and constant κ are plotted in the vicinity of the airfoil after throwing away the solution in which $V_t<0$.

To examine how the pressure distribution on the airfoil is affected by the external vortex, we first find the velocity V on the airfoil surface from transformation of the velocity on the circle in the ζ' plane using Eq. (8). The pressure coefficient, which is defined as the pressure difference between the local and a far-away station divided by the dynamic pressure at infinity, is then computed from the formula

$$C_p=1-(V/U)^2 \quad (30)$$

The stream function is the imaginary part of the complex potential shown in Eq. (7). The method described in Ref. 7 is used to plot the streamlines and pressure distribution around the airfoil.

Applying the Blasius theorem to the present problem having a vortex outside the airfoil, we obtain a lift of $\rho U(\Gamma+\kappa)$ per unit span of the wing. We define L as this lift divided by ρU, so that

$$L=\Gamma+\kappa \quad (31)$$

VI. Stability of the Free Vortex

The equilibrium position of the free vortex at which the vortex becomes stationary has been found. Extending the analysis of Saffman and Sheffield[5] for a flat plate, we will examine the stability of the vortex when it is perturbed from the equilibrium position near an airfoil. The analysis is simplified by assuming two-dimensional disturbances of small amplitudes, and by ignoring the shed vortices in the wake after being disturbed so that the free vortex and bound vortex remain their original strength κ and Γ, respectively.

The complex velocity of the free vortex is, from Eq. (11),

$$u-iv=\frac{\zeta^2}{\zeta^2-1}\left[e^{-i\alpha}-\left(\frac{a}{\zeta'}\right)^2 e^{i\alpha}-\frac{i\kappa}{\pi}\frac{1}{\zeta'-a^2/\bar{\zeta}'}\right.$$
$$\left.+\frac{i}{\pi}\frac{\Gamma+\kappa}{\zeta'}\right]-\frac{i\kappa}{\pi}\frac{\zeta}{(\zeta^2-1)^2}=Q(\zeta',\bar{\zeta}') \tag{32}$$

in which ζ and ζ' are related through Eq. (2), and $Q(\zeta_0',\zeta_0')=0$ in the equilibrium position $\zeta'=\zeta_0'$. For a small displacement ζ_1' away from the equilibrium point ζ_0', we have

$$\frac{d\bar{\zeta}_1'}{dt}=\frac{d\bar{\zeta}_1'}{d\bar{z}}\frac{d\bar{z}}{dt}=\frac{d\bar{\zeta}_1'}{d\bar{z}}Q(\zeta',\bar{\zeta}')$$

Taylor's expansion about ζ_0' results in

$$\frac{d\bar{\zeta}_1'}{dt}=A\zeta_1'+B\bar{\zeta}_1' \tag{33}$$

where

$$A=\left(\frac{\partial Q}{\partial\zeta'}\frac{d\bar{\zeta}}{d\bar{z}}\right)_{\zeta_0'} \qquad B=\left(\frac{\partial Q}{\partial\bar{\zeta}'}\frac{d\bar{\zeta}}{d\bar{z}}\right)_{\zeta_0'} \tag{34}$$

For solutions of Eq. (33) having the form $e^{\sigma t}$, we must have

$$\sigma^2-(B+\bar{B})\sigma+B\bar{B}-A\bar{A}=0 \tag{35}$$

It turns out that B is purely imaginary so that $B+\bar{B}=0$. Instability occurs when σ has a positive real part. Thus a stability condition is deduced from Eq. (35) which requires that

$$|B|\geq|A| \tag{36}$$

The complex expressions for A and B are obtained in a straightforward manner after differentiating Eqs. (1) and (32).

VII. Results for the Flat Plate

It can be shown that our analysis reduces to that of Saffman and Sheffield[5] for a flat plate by letting $\delta=0$. The results presented in this section are merely used to complement their previous work.

The equilibrium positions (x_0, y_0) of the free vortex are plotted in Fig. 3 for both constant α and constant κ. There are two regions in which a vortex can be captured; the area of the leading-edge region is much larger than that of the trailing-edge region. However, the vortex is unstable at all loci except at those along the upper portion of the $\alpha=5$-deg curve above the point marked by a cross near the trailing edge. Of course there exist other stable loci for angles of attack in the neighborhood of 5 deg. For example, the case of $\alpha=0.1$ rad (or 5.73 deg) is presented in Ref. 5. The figure also reveals that stronger vortices can be captured only at distances farther away from the flat plate.

The sum $\Gamma+\kappa$, which is proportional to the lift, is plotted against y_0 in Fig. 4 for constant values of α. Each of the curves is cut off when $V_t=0$, that is, when the trailing edge becomes a stagnation point. The cut-off point represents the maximum vortex lift that the flat plate can attain at a given angle of attack; whereas the lowest point on the same constant α curve, which occurs at $y_0=0$ when $\kappa=0$, represents the lift in the absence of an external vortex. The plot shows that the leading-edge vortices are more effective in generating lift, but unfortunately they are not stable to small disturbances. Nevertheless, considering the stable loci near the trailing edge at 5 deg angle of attack, the maximum vortex-augmented lift is about ten times the original lift on the flat-plate airfoil.

Plots of some representative streamline patterns and pressure distributions are referred to in Ref. 5.

VIII. Results for Symmetric Airfoils

With $\mu=\pi$, several symmetric airfoils have been constructed by varying δ. Presented first are the results for the airfoil with $\delta=0.15$, whose shape is shown in Fig. 5 having a chord of 2.035.

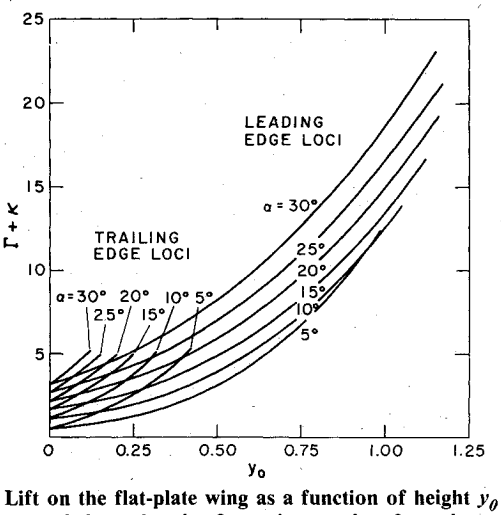

Fig. 4 Lift on the flat-plate wing as a function of height y_0 of the vortex captured above the wing for various angles of attack.

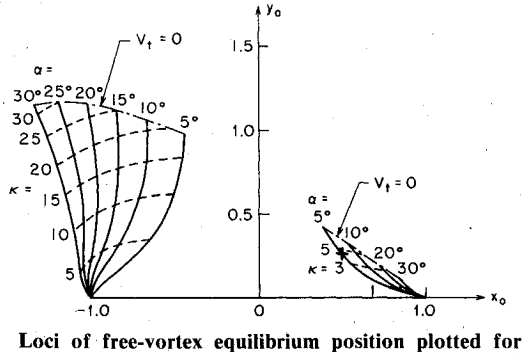

Fig. 3 Loci of free-vortex equilibrium position plotted for both constant α and constant κ for the flat-plate wing; the vortex is stable along the $\alpha=5$ deg curve above the point marked by a cross.

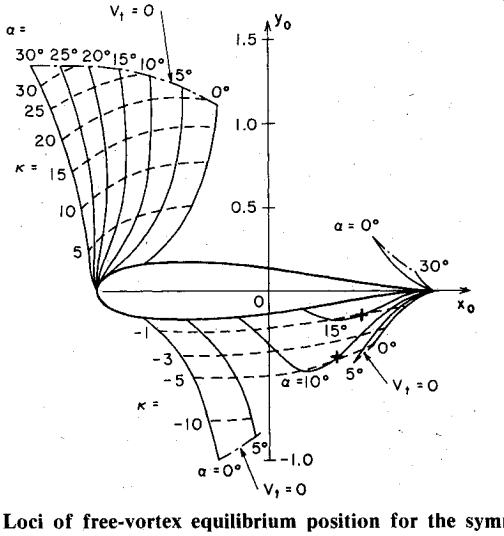

Fig. 5 Loci of free-vortex equilibrium position for the symmetric airfoil with $\mu=\pi$ and $\delta=0.15$. Below the trailing edge, the vortex is stable on the entire $\alpha=0$- and 5-deg curves and to the right of the cross on $\alpha=10$- and 15-deg curves.

Loci of free-vortex equilibrium positions plotted in Fig. 5 show that, for positive angles of attack, vortices of clockwise and counterclockwise circulations can be trapped above and below the wing, respectively. This property is different from that of the flat plate, below which no vortex can be trapped. A blown-up plot of the region above the trailing edge is shown in Fig. 6. The vortex is still unstable in the leading-edge region either above or below the airfoil, but may become stabilized near the trailing edge. Increasing angle of attack has a destabilizing effect, and the area occupied by the stable loci above the airfoil is much larger than that above the flat plate.

The lift as a function of height y_0 is plotted in Fig. 7 for vortices trapped above the wing, and in Fig. 8 for those trapped below it. For vortices above the wing, the general trend is that the maximum lift generated from a leading-edge position of the symmetric airfoil is higher than that of the flat plate at the same angle of attack, whereas the opposite is true considering the trailing-edge positions. Figure 8 shows that lift decreases when a vortex of counterclockwise circulation is trapped below the wing. Such a case therefore is not interesting for practical applications.

A representative flow pattern with a vortex trapped in a leading-edge position is shown in Fig. 9, plotted for the arrangement that the vortex is at the point $(-0.631, 0.515)$ and the angle of attack is 5 deg. The corresponding pressure distribution on the surface of this airfoil is plotted in Fig. 10 to compare with that on the same airfoil but without the external vortex. It shows that on the upper surface of the airfoil, there exists an extremely low-pressure region below the vortex, which is followed by a high-pressure region up to the trailing edge. The pressure change on the lower surface of the airfoil caused by the vortex is relatively small. The vortex-augmented lift, which is 2.27 times the lift of the airfoil in the absence of the vortex, is mainly attributed to the low pressure under the vortex. Note that a strong nose-up moment about the midchord results from such a pressure distribution.

Figure 11 depicts the flow pattern when a vortex of coordinates (0.746, 0.180) becomes stationary near the trailing edge of the airfoil at $\alpha = 5$ deg. A stagnation point occurs at the trailing edge, corresponding to the maximum-lift arrangement for that angle of attack. The pressure distribution on the surface is plotted in Fig. 12. The extremely low-pressure region below the vortex still appears in addition to the low-pressure region near the leading edge on the upper surface. In this case the moment about the midchord is in the nose-down sense.

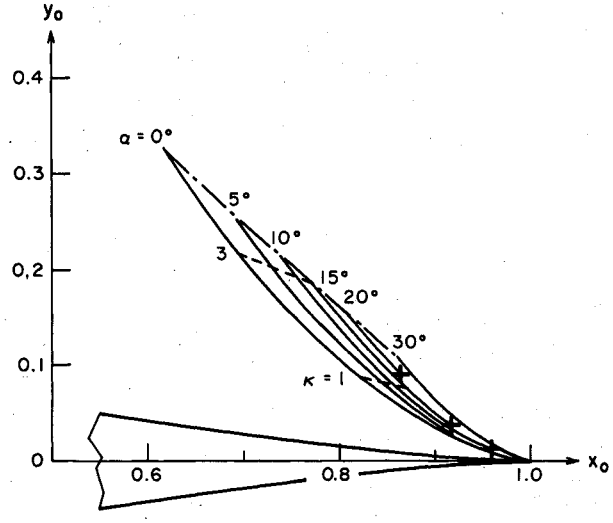

Fig. 6 Blown-up view of the region above trailing edge of Fig. 5. The vortex is stable on the entire $\alpha = 0$-deg curve and above the point marked by a cross on each of the other constant α curves. The cross on the $\alpha = 5$-deg curve, being very close to the trailing edge, is not shown. It is unstable on the entire $\alpha = 30$-deg curve.

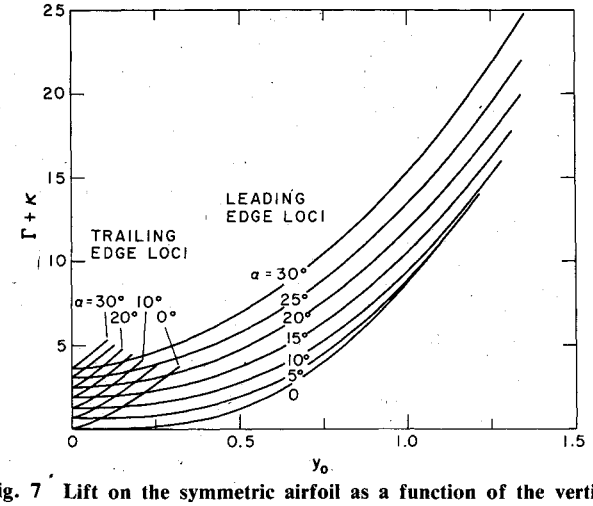

Fig. 7 Lift on the symmetric airfoil as a function of the vertical coordinate y_0 of the vortex captured above the wing for various angles of attack.

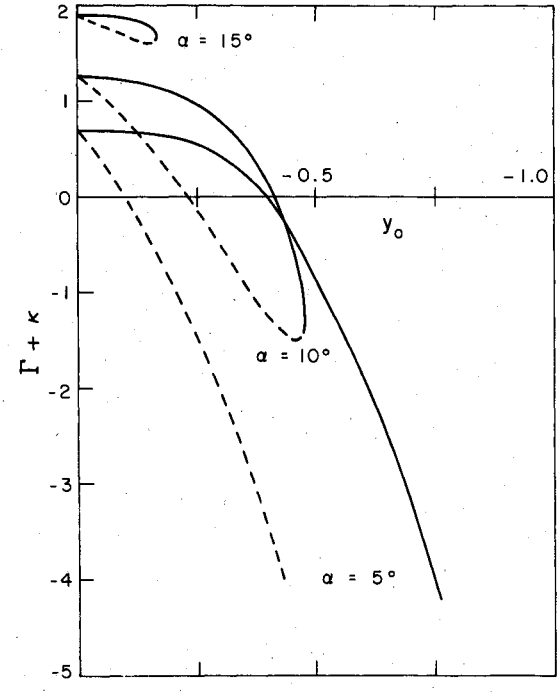

Fig. 8 Lift on the symmetric airfoil as a function of the vertical coordinate y_0 of the vortex captured below the wing for various angles of attack. Solid lines are for the leading-edge loci and dashed lines are for the trailing-edge loci.

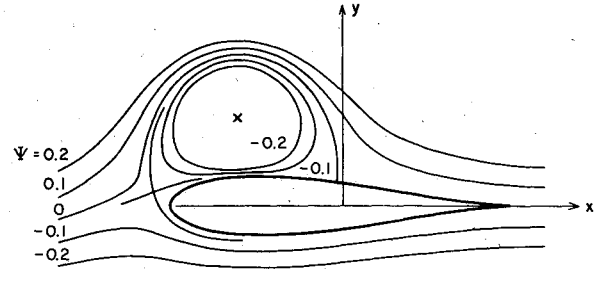

Fig. 9 Streamline pattern for vortex of coordinates $(-0.631, 0.515)$ on leading-edge locus of symmetric airfoil ($\mu = \pi$, $\delta = 0.15$) at 5-deg angle of attack.

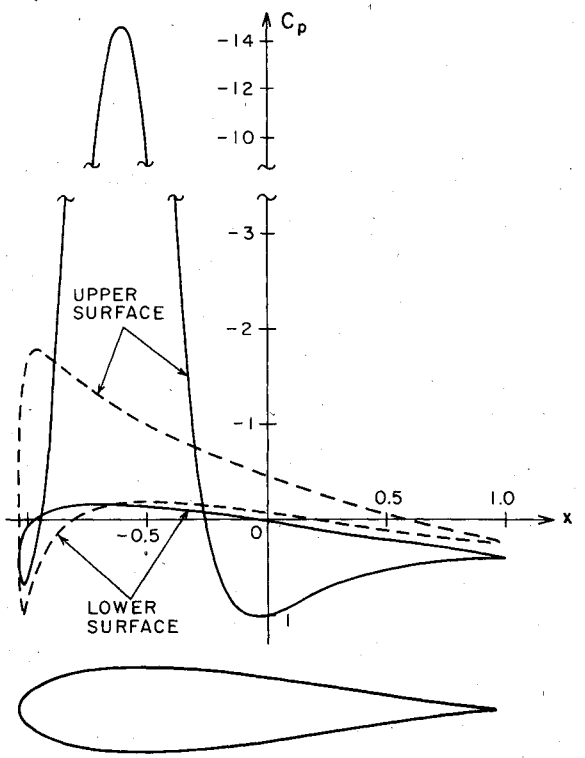

Fig. 10 Pressure distribution on the airfoil described in Fig. 9 (solid curve) in comparison with that on the same airfoil in the absence of an external vortex for $\alpha = 5$ deg (dashed curve).

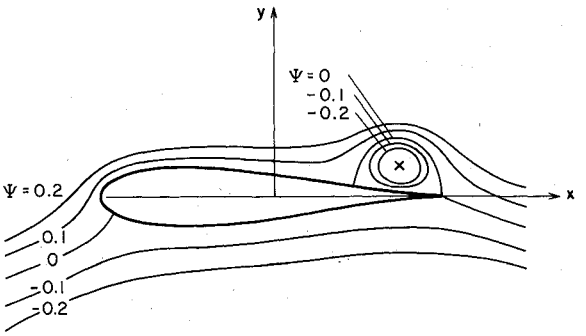

Fig. 11 Streamline pattern for vortex of coordinates (0.746, 0.180) on trailing-edge locus of a symmetric airfoil ($\mu = \pi$, $\delta = 0.15$) at 5-deg angle of attack.

Keeping $\mu = \pi$ but decreasing δ from 0.15 to 0, a series of symmetric airfoils of almost the same chord but of decreasing thickness is generated. Based on the computations for a constant angle of attack of 0.1 rad, Fig. 13 shows that with decreasing thickness, the trailing-edge stability range shortens, the maximum lift on the leading-edge locus decreases whereas that on the trailing-edge locus increases. In other words, a thicker airfoil has a higher ability of stably trapping a vortex on the upper surface, but the price paid for this advantage is the lower maximum lift that can be generated on the wing.

IX. Results for Circular-Arc Airfoils and Cambered Airfoils

The transformations Eqs. (1) and (2) map the circle in Fig. 2 into a circular arc if $\mu = \pi/2$, whose curvature increases with increasing δ. The results obtained for four values of δ are presented in Fig. 14 at $\alpha = 0.1$ rad. As the curvature (or the camber) of the circular-arc airfoil increases, the maximum lift on the leading-edge locus increases but that on the trailing-edge locus decreases. No stability locus is found near the

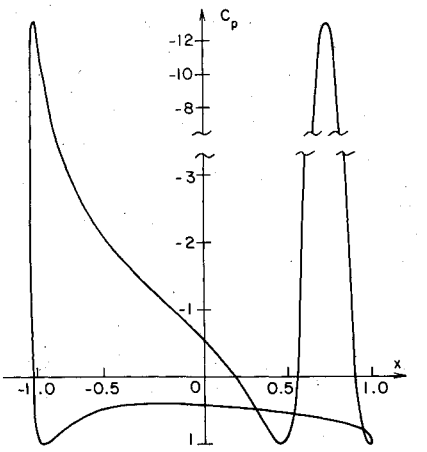

Fig. 12 Pressure distribution on the airfoil described in Fig. 11.

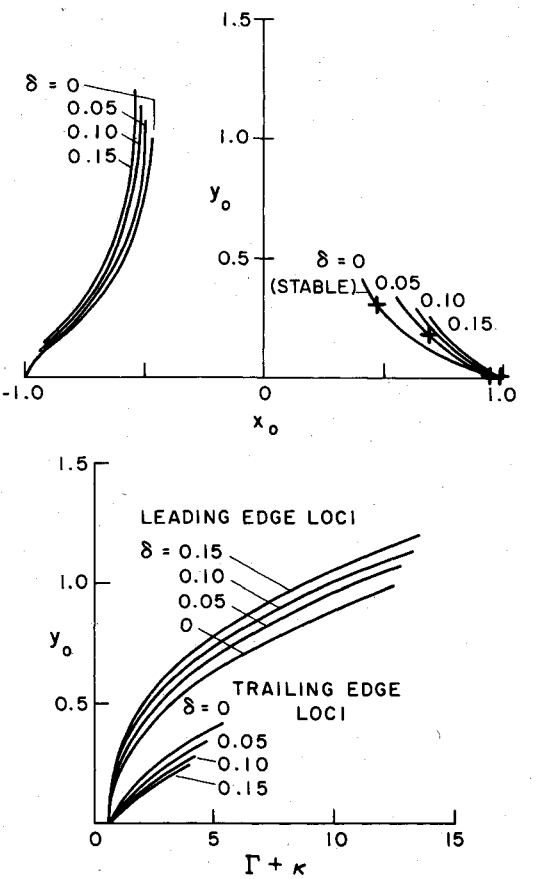

Fig. 13 Loci of free vortex and lift for symmetric airfoils of different thickness at $\alpha = 0.1$ rad.

leading edge for all values of δ. Near the trailing edge, however, there is a short stability range on the loci for the flat plate with $\delta = 0$, while the loci for the three nonvanishing values of δ that we have chosen are all unstable.

Cambered airfoils of almost the same thickness are constructed from mapping of the circle in Fig. 2 by varying the angle β while keeping the radius a at a constant value of, say, 1.15. A higher value of β gives a larger camber and a slightly shorter chord. For given values of a and β, the corresponding values of δ and μ needed in the computation are obtained from Eqs. (3) and (4). The conclusion on the variation of the maximum lift with camber is the same as that for circular-arc airfoils, which are in fact cambered airfoils of vanishing thickness, as shown in Fig. 15 for $\alpha = 0.1$ rad. The trailing-

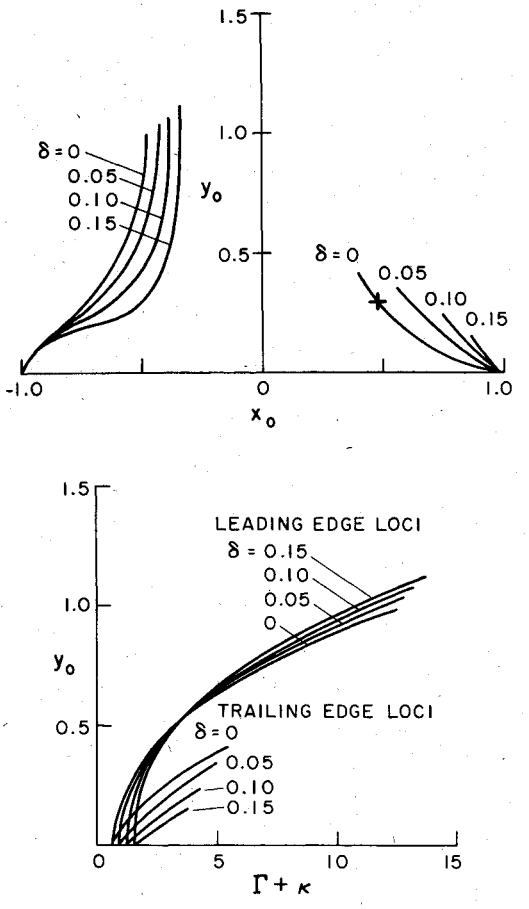

Fig. 14 Loci of free vortex and lift for circular-arc airfoils of different camber at $\alpha = 0.1$ rad.

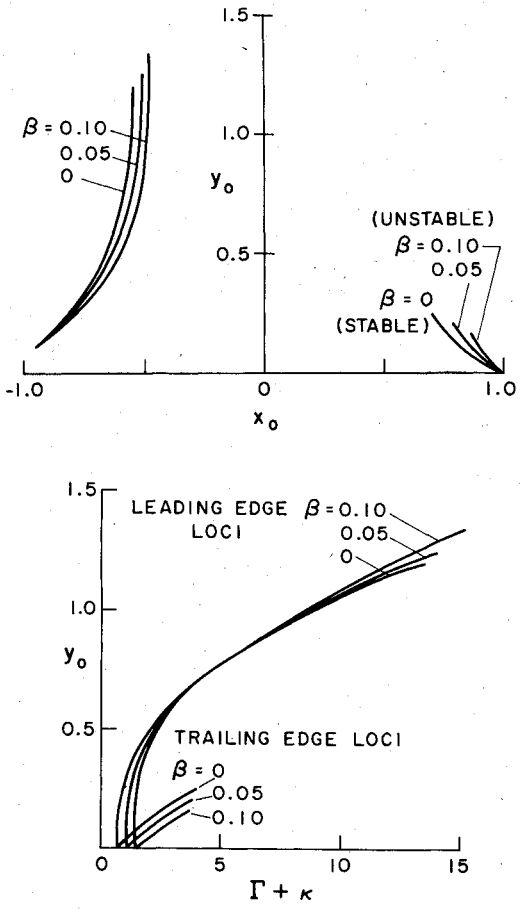

Fig. 15 Loci of free vortex and lift for cambered airfoils of almost the same thickness ($a = 1.15$) but different camber at $\alpha = 0.1$ rad.

edge loci are stable for $\beta = 0$ (symmetric airfoil), and are unstable for both $\beta = 0.05$ and 0.1.

Combining these two sets of results, we can say that for a fixed thickness, either vanishing or finite, the camber decreases the ability of the airfoil to stably trap a vortex near the trailing edge. A small camber may make all equilibrium positions of the free vortex unstable.

X. Conclusions

To summarize the results presented in the previous sections for airfoils of various geometries, we make the following conclusions.

1) Although very high lifting forces can be generated by a stationary vortex captured above the leading edge, the vortex is always unstable in the sense that the vortex will move away after being displaced slightly from its equilibrium position. From the cases that have been considered, this conclusion seems to be true independent of both the thickness and camber of the airfoil.

2) A free vortex may become stably trapped above the trailing edge for lift generation according to a linearized stability analysis for two-dimensional disturbances. The maximum lift that can be generated by a stable trailing-edge vortex is generally several times higher than the lift on the same airfoil without an external vortex, even if it is small in comparison with the maximum lift generated by the leading-edge vortex. The vortex trapped below the airfoil has an opposite effect of decreasing the lift of the airfoil.

3) Increasing angle of attack diminishes the vortex-trapping ability of the airfoil and reduces the magnitude of the maximum lift that can be produced by the stable vortices. For a given airfoil, no vortex can be captured if the angle of attack exceeds a limiting value.

4) The effect of increasing thickness is to stabilize the trailing-edge vortex but in the meantime to reduce the maximum lift of the airfoil.

5) The effect of increasing camber is similar to that of increasing angle of attack as far as the stability and maximum lift are concerned. It has such a particularly strong destabilizing effect that a small camber may cause all equilibrium positions of the vortex to become unstable.

6) For the purpose of increasing the lift of a wing by utilizing a trapped external vortex, it is appropriate to use a reasonably thick symmetric airfoil at a small angle of attack. The conclusion is made based on the analysis for a two-dimensional potential flow model.

Acknowledgment

This work was supported by the Air Force Office of Scientific Research under Grant AFOSR 81-0037.

References

[1] Cox, J., "The Revolutionary Kasper Wing," *Soaring*, Vol. 37, Dec. 1973, pp. 20-23.

[2] Walton, D., "A Brief Wind Tunnel Test of the Kasper Airfoil," *Soaring*, Vol. 38, Nov. 1974, pp. 26-27.

[3] Kurppa, E. W., "A Wind Tunnel Investigation of the Kasper Vortex Concept," AIAA Paper 77-310, Jan. 1977.

[4] Rossow, V. J., "Lift Enhancement by an Externally Trapped Vortex," AIAA Paper 77-672, June 1977.

[5] Saffman, P. G. and Sheffield, J. S., "Flow over a Wing with an Attached Free Vortex," *Studies in Applied Mathematics*, Vol. 57, 1977, pp. 107-117.

[6] Sheffield, J. S., "Topics in Vortex Motion," Ph.D. Thesis, California Institute of Technology, 1978.

[7] Chow, C.-Y., *An Introduction to Computational Fluid Mechanics*, 1st ed., Wiley, New York, 1979, Sec. 2.7.